JOURNAL OF GEOPHYSICAL RESEARCH, VOL. 101, NO. D2, PAGES 4351–4362, FEBRUARY 20, 1996

Lagrangian evolution of an aerosol column during the Atlantic Stratocumulus Transition Experiment

Antony D. Clarke, Tomoe Uehara, and John N. Porter

School of Ocean and Earth Science and Technology, University of Hawaii, Honolulu

Abstract. Two Lagrangian experiments were carried out during the Atlantic Stratocumulus Transition Experiment (ASTEX) with the intent of looking at aerosol evolution in the marine boundary layer (MBL). The second Lagrangian (L2) took place below broken stratus clouds and was more successful since little precipitation reached the surface. Aerosol below the inversion was primarily an aged pollution aerosol from central Europe. Vertical variability in aerosol concentrations was generally characterized by highest concentrations in the moist surface and transition layers. Concentrations were a factor of 2 or more lower in the dry subcloud layer and cloud layer and dropped to less than one tenth of surface values in the free troposphere above cloud. This behavior reflected the decoupled boundary layer below the main inversion and complicated the assessment of Lagrangian aerosol evolution. No evidence for new particle formation was observed during L2, and aerosol evolution proceeded only by mixing, coagulation, and removal mechanisms. An entrainment rate of about 0.6 cm s^{-1} from the free troposphere into the MBL was a key parameter affecting aerosol evolution and resulted in about a 35% column dilution during the 34-hour L2 measurement period. Aerosol evolution in the decoupled subcloud and surface marine layer is consistent with an entrainment rate of about 0.45 cm s^{-1} into the surface layer and about 0.25 cm s^{-1} out of the layer. The ability to resolve the effects of separate processes influencing both gas and aerosol during Lagrangian evolution will depend upon (1) an adequate assessment of the variability in the air mass, (2) the ability to characterize this variability relative to the uncertainties in resampling the air mass, and (3) the extent to which the substantial changes due to entrainment alone can be reliably determined.

1. Background

The atmospheric aerosol is of current interest due to its role (1) as a transient atmospheric reservoir in the geochemical cycling of numerous species (e.g. soot, sulfur, ammonia), (2) in the modulation of the radiative transmission (scattering and absorption) of the atmosphere for both natural and artificial light sources, and (3) in affecting cloud properties (optical reflectivity, precipitation process, etc.) sensitive to the size and composition of particles activated as cloud condensation nuclei. Various scientific concerns related to these properties include (1) the budgets and lifetimes of anthropogenic and natural emissions [*Galloway et al.*, 1985], (2) effects upon radiative transfer from pollution-derived sulfate [*Charlson et al.*, 1992] and/or (3) the influence on cloud albedo [*Charlson et al.*, 1987], (4) acid rain/deposition [*Galloway et al.*, 1982] and (5) visibility impairment [*Air and Waste Management Association*, 1994].

The lifetime of aerosol in the lower troposphere is of the order of a day to a week and considered to be largely determined by removal via precipitation [*Galloway et al.*, 1985]. This lifetime is sufficient for aerosol to be carried over hundreds to thousands of kilometers by ambient winds. Interest in the relative influence of anthropogenic versus natural emissions has prompted the inclusion of parameterized source, transformation, and removal mechanisms for aerosol into large-scale global circulation models (GCM). A recent example of this is the estimation of anthropogenic sulfate emissions over the Atlantic region [*Benkovitz et al.*, 1994]. The parameterizations often used in such models are based upon current best estimates of aerosol transformation and removal mechanisms. It is expected that satellite retrieval algorithms for aerosol column properties will be refined and eventually linked with these models as a means of studying these issues on a global scale [*Penner et al.*, 1993]. The validation of both model performance and/or satellite retrievals will require in situ evaluations of the key processes that determine column aerosol evolution. However, few experiments have tested the evolution of gas and aerosol species in a Lagrangian reference frame. This is largely due to the difficulty and effort required to carry out such an experiment, including the need for aircraft to establish an adequate database throughout the vertical column of air under study. The direct measurement of the Lagrangian evolution of an aerosol, such as we describe here, is an approach for assessing the key parameters needed for refinement of current models and for the improved interpretation of satellite retrievals.

Copyright 1996 by the American Geophysical Union.

Paper number 95JD02612.
0148-0227/96/95JD-02612$05.00

2. Instrumentation

Our principal instrumentation included a laser optical particle counter (OPC) with a dilution drier and thermal volatility [*Clarke.*, 1991], a differential mobility analyzer (DMA, Thermo Systems Inc., TSI 3071) with thermal volatility, condensation nuclei (CN, TSI 3760) counters, an ultrafine condensation nuclei (UCN, TSI 3025) counter, and an aethaelometer (Magee Scientific) for the inference of aerosol light absorption and black carbon (BC) concentration. More complete instrument specifications can be found elsewhere (A.D. Clarke et al., Properties of aerosol fields over the Atlantic: Clean and polluted air during ASTEX, submitted to *Journal of Geophysical Research*, 1995; hereafter referred to as submitted manuscript, 1995). The thermal volatilization approach refers to the measurement of ambient aerosol after drying to about 20% relative humidity and heating to three temperatures (40°, 150°, 300°C) with 40°C considered to be the "ambient" standard measurement. Mass lost during heating to 150°C is presumed to be sulfuric acid in clean marine air (also possibly organic material or nitrates in polluted air) while all volatile material lost by 300°C includes ammonium sulfate/bisulfate leaving a "refractory" residual aerosol. This refractory component originates primarily from surface processes (sea salt, dust, or black carbon derived from combustion processes). This volatility technique enables rapid inference of the size-resolved aerosol composition over timescales of several minutes, required when a variable air mass is measured from aircraft traveling at 6 km min^{-1}. Volatility is also used as a basis for characterizing properties of the aerosol number population. Two CN counters were operated at cabin temperature and 300°C to provide total CN (D_p>15 nm) and refractory CN (RCN) respectively. The ratio of refractory RCN to CN is a useful "normalized" indicator (A.D. Clarke et al., submitted manuscript, 1995) of air mass character (e.g., clean versus polluted) with real-time (1 Hz) measurement capability. This combination of fast-response and size-resolved volatility instrumentation provides complementary information on the physical, chemical, and optical properties of the aerosol. Comparison of the evolution of these properties during L2 will be discussed here.

3. ASTEX Lagrangian 2

3.1. Characteristics of the Aerosol Field

Our participation in the second Lagrangian (L2) of the Atlantic Stratocumulus Transition Experiment (ASTEX) took place aboard the National Center for Atmospheric Research (NCAR) Electra aircraft, which flew primarily in polluted air of European origin. The trajectory of the air mass, the flight locations of the aircraft, and description of the general conditions can be found in a companion paper in this issue [*Huebert et al.*, this issue]. The aircraft flew four missions over a 34-hour period that were designed to sample the same column of air. Locating the same position in the air mass was established relative to balloons launched to advect with the air mass [*Businger et al.*, this issue]. Aerosol data were obtained during flights 11 (June 18, 1992), 12 (June 19, 1992), 13 (June 19, 1992), and 14 (June 20, 1992). Each flight consisted of two sequences of 4-6 stacked 30-min L-shaped "legs" extending from the surface up to the free troposphere. Typically, one side of the L was flown across wind and the other parallel to the wind for about 15 min each. These Ls were continuously "advected" with the wind. An exception was flight 12, which flew all 30 min cross-wind legs due to a miscommunication about balloon location [*Huebert et al.*, this issue].

The vertical structure in the decoupled marine boundary layer (MBL) at the beginning of L2 has been described as a well-mixed moist surface mixed layer (SML 0-300 m) below a transition layer (TL 300-700 m) lying beneath a dry subcloud layer (SCL 700-1350 m) topped by a cloud layer (CL 1350-2000 m) that was separated from the free troposphere (FT) by the main inversion [*Martin et al.*, 1994]. The TL often had a complex fine-scale layered structure in potential temperature suggesting alternating mixed layers originating from both the SML and SCL. The thermodynamic structure of the area suggested that cumulus towers of the order of 1 to 2 km diameter originating from the SML could penetrate through the TL and SCL to form anvils in the CL and feed the stratocumulus with SML air and aerosol [*Bretherton and Pincus*, 1994; *Martin et al.*, 1994]. Light drizzle was observed below clouds on L2, particularly the morning of June 19, but most was found to have evaporated before reaching the ground [*Bretherton et al.*, 1994], and little drizzle was observed for the rest of L2. An extensive discussion of the air mass properties, synoptic setting, cloudiness and drizzle, etc., can be found elsewhere [*Martin et al.*, 1994; *Bretherton and Pincus*, 1994; *Bretherton et al.*, 1994].

Two examples of vertical profiles from L2 are shown in Figure 1 for flights 13 and 14. These reveal the meteorological (RH, potential temperature), ozone and aerosol (CN, BC) vertical structure, and related changes after about 12 hours. Approximate locations for the different layers discussed above are indicated. Both coarse and fine-scale features are evident as well as related variability in aerosol and meteorological fields. On flight 13 (top) the CN suggest two well-mixed layers with concentrations of about 2000 cm^{-3} near the surface up to 500 m and about 1300 cm^{-3} in the TL up to 1000 m. Potential temperature and ozone also indicate well-mixed layers at this time. Twelve hours later (bottom) on flight 14 the concentrations have dropped in both layers and stronger gradients have developed along with more variability in the meteorological parameters. The variability in BC is similar on both days and indicates that pollution is present up to 4500 m but with some what "cleaner" air in the dryer region at 2000-3000 m. Some problems with this measurement during rapid pressure changes (A.D. Clarke et al., submitted manuscript, 1995a) make these BC profiles more uncertain.

In order to interpret changes in any aerosol parameter measured during a Lagrangian experiment one must have information on the spatial variability of the aerosol field under study. The National Center for Atmospheric Research (NCAR) Electra flying at 100 m/s covers about 6 km each minute such that sampling on the order of seconds is needed to obtain even kilometer-scale information on spatial variability. This variability can be large both within a specific aerosol field (e.g., pollution) and in transition regions between fields (A.D. Clarke et al., submitted manuscript, 1995a). The most rapid aerosol measurement capturing this variability was for CN, recorded at 1 Hz but grouped into 15-s averages for the data shown here. Representative examples of this variability along a leg are shown in Figure 2 for CN D_p>0.015 μm, refractory CN (RCN at 300°C), and ultrafine CN (UCN, all particles 0.003<D_p<3 μm) concentrations along with the dimensionless RCN/CN ratio. This is done for each flight and for comparable altitudes flown in the well-mixed SML, the TL, and the SCL. Due to

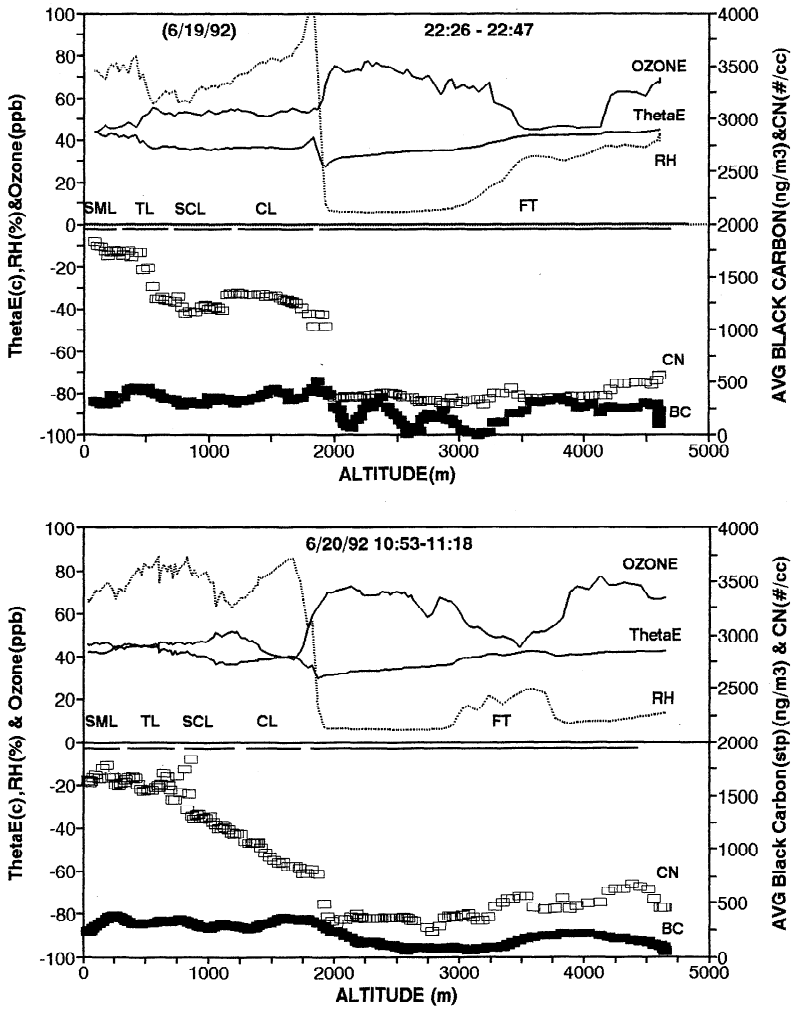

Figure 1. An example of vertical structure found during the ASTEX second Lagrangian for ozone, potential temperature, relative humidity, condensation nuclei and black carbon. Layer characterization after *Martin et al.* [1994] (see text).

space limitations, data are presented from only of one of the two stacks flown on each flight. However, due to variable conditions for each flight, these legs were not flown at identical altitudes (see notation on figures) but have been selected to best represent the same layer. The RCN/CN ratio is also plotted as a "normalized" indicator of air mass "character", since it is relatively insensitive to concentration changes but varies with the "mix" of aerosol types. In polluted regions the ratio tends to 1, and in "clean" regions it tends to 0 (A.D. Clarke et al., submitted manuscript, 1995a).

Lagrangian flight legs attempted to position the "balloon" near the midpoint of an imaginary line connecting both "ends" of the L-shaped legs. In Figure 2 the superposition of the balloon is based upon projecting its position along the mean wind and onto the cross-wind part of the leg. The "turn" point of the L is also indicated and, because the westernmost part of the L was oriented in more of a north-south direction, it projects out of the page and appears much "shorter" in this presentation. Also, because the winds vary about a southerly direction during the course of L2 [*Businger et al.*, this issue], the projection of the westernmost downwind leg appears somewhat different in each figure. Recall that flight 12 was entirely across wind and not an L pattern.

Figure 2 reveals a number of features in the CN data that should be considered in selecting appropriate data for a Lagrangian assessment.

1. The CN data describes the detailed structure in the aerosol fields that cannot be obtained for many other aerosol measurements such as aethaelometer data and filter samples [*Huebert et al.*, this issue].

2. The CN, RCN, and UCN all decrease significantly over the L2 time period at all altitudes. The absence of appreciable new particle formation in the evolving pollution plume and the fact that the RCN/CN ratio decreases to slightly lower values during L2 at each higher altitude suggests the steady mixing (entrainment) with air having a lower concentration of CN and lower RCN/CN ratio, as discussed below.

3. Steep gradients in CN concentrations are most conspicuous in the westernmost end of the legs, a region that is associated with more cloudiness (see "spikes"-droplet shatter). Spikes in the data show up with almost equal amplitude in the RCN and CN. This occurred whenever the liquid water content exceeded about 0.02 g kg^{-1} and is caused by droplet shatter on our sampling probe inlet and does not reflect localized high particle concentrations. Larger cloud/drizzle droplets in the marine environment nearly always include sea salt (refractory

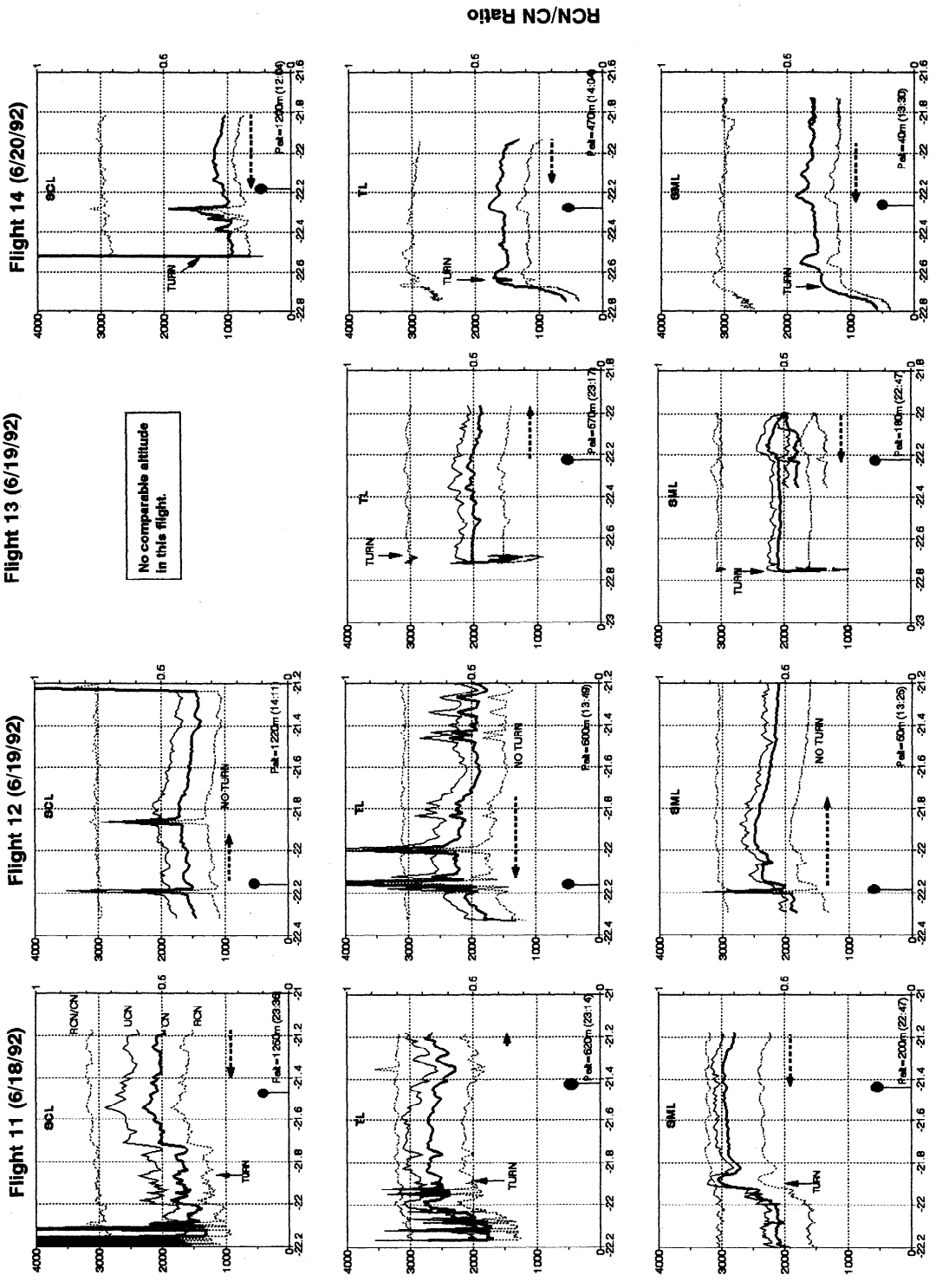

Figure 2. Representative plots of UCN, CN, RCN, and RCN/CN as a function of longitude along representative sample legs for each of the Electra flight days flown during L2. The projected reference position of the balloon is indicated along with the location of the "turn" during the L shaped legs. Although the time duration on either side of the turns was the same, the westernmost portion was flown in a more N-S direction and appears compressed in this presentation. Upper panels are for the subcloud layer (SCL), middle panel for the transition layer (TL), and lower panels for the surface mixed layer (SML) although the same altitudes were not exactly maintained from flight to flight (see text for details).

at 300°C) that, upon shattering, produces numerous smaller droplets containing sea salt. Upon drying, these yield the characteristic spike in both CN and RCN shown (A.D. Clarke et al., submitted manuscript, 1995a). The more frequent spikes for flight 11 and 12 are consistent with the more frequent drizzle for that period [*Bretherton et al.*, 1994].

4. Because downwind legs were unintentionally flown near or in the air mass boundary, the variability along the main plume axis was not well characterized during L2. However, some indication of this structure can be seen from the SML data shown for flight 13. Here we have included data for the initial approach to the eastern start (at 22°W) of the leg (180-m altitude) from a position upwind and at about a 30° angle to the leg. A comparison of concentrations before and after the turn reflect a 10-20% difference in all nuclei concentrations corresponding to about 10-20 km in downwind displacements. The absence of a change during the turn confirms that this difference is not an aircraft sampling artifact.

5. The RCN/CN ratio is high (~ 0.8) for this polluted air mass, reflecting an aerosol that includes a refractory sootlike residual that remains after removing volatile mass (e.g., sulfate) at 300°C (A.D. Clarke et al., submitted manuscript, 1995a).

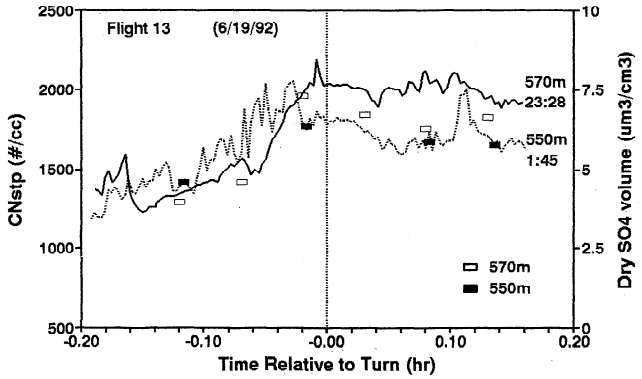

Figure 3. A comparison of the time series for the continuous CN data shown in Figure 2 for flight 13 at 570 m and the subsequent flight about 2.2 hours later at 550 m plotted relative to the turn in the L shaped legs. OPC inferred fine particle volume is plotted as boxes for approximately 1-min unheated periods. This presentation reveals the aerosol gradient along the westernmost part of both legs. The structure is repeated for both legs and shows similar variability for both instruments.

3.2. Spatial Variability

The data shown in Figures 1 and 2 clearly indicate regions that include both significant horizontal gradients and vertical gradients in aerosol concentrations. Careful positioning of the aircraft relative to the balloon needed to be be carried out in all three dimensions. The problem of representative sampling is also constrained by the limited number of altitudes that can be realistically flown and the practical need to deviate from intended altitudes due to in-flight considerations such as the location of low-level "scud" clouds. It is this complexity that makes the interpretation of L2 data difficult and introduces uncertainties. Even with continuous characterization (eg. CN counters), the appropriate spatial scale for averaging data needs to be small enough to avoid large-scale gradients and large enough to average over small-scale variability Consequently, the evaluation of trends during L2 aerosol evolution require proper selection, appropriate averaging, and the identification of changes originating from instrument uncertainty, positioning uncertainty, or atmospheric variability.

The significance of atmospheric variability for the OPC and CN measurements is illustrated in Figure 3. Here we have taken the same CN data (solid line) shown in Figure 2 for flight 13, leg 3 (570 m) but shown here as a function of time before and after the turn in the L in order to better reveal the downwind data, which appear compressed in Figure 2. The CN data for the next most comparable altitude flown about 2 hours later (flight 13, leg 8) at 550 m is also shown (dashed line). Although similar gradient and structure are present in CN for both legs, the concentrations are lower on the west end and higher on the east end for the 550-m altitude than for the 570-m altitude. Aerosol fine particle dry volume, inferred from the 1-min OPC data after correcting for residual water based upon aerosol volatility [*Clarke*, 1991] and a presumed composition like ammonium bisulfate (see below), has been superimposed on the CN data (Figure 3) for comparison. This OPC-derived dry volume (hereafter referred to as OPC dry sulfate, see below) follows CN variability closely and with the same tendency for higher and lower values on both legs. This behavior indicates that (1) the variabilities in the number of CN and OPC mass are consistent with each other; (2) differences in the spatial horizontal structure of the aerosol are much greater than uncertainties in measurement precision of either CN or OPC data; and (3) short temporal changes and small vertical displacements involve significant aerosol variability that can be resolved by these instruments. This means that these instruments are appropriate for looking at the changes in aerosol evolution but that selection of the spatial and temporal averages used for the assessment and interpretation of Lagrangian evolution must be made with care.

The time series format employed in the discussion of the Lagrangian data to follow does not reveal the aerosol vertical structure. Consequently, the OPC dry volumes for the four flights have been plotted as vertical profiles in Figures 4a and 4b. Figure 4a shows the OPC dry volume concentration as a function of altitude, and superimposed upon the plot are the various layers as defined previously. Notice that the structure revealed here for fine particle volume is consistent with that illustrated by the CN data in Figure 1. The time evolution (decrease) of the OPC concentrations is also apparent. It is also evident from this and the previous figures that both the number of legs flown and the choice of altitudes were not adequate to fully characterize the aerosol column and its evolution in this decoupled system.

We have also used OPC thermal volatility to infer the variability in the relative amounts of sulfuric acid and ammonium sulfate in the aerosol [*Clarke*, 1991] in order to estimate a molar ratio of $NH_4^+/SO_4^=$ in the aerosol as shown in Figure 4b. If low-temperature organic material were present and volatile below 150°C, then the real ratio would be higher than shown here. Since our dry sulfate volume inferred from OPC volatility agrees within about 20% of the values measured directly [*Zhuang and Huebert*, this issue], we think that it is unlikely that organic material will exceed 20% of the fine particle mass, and it may be less. Our inferred near-surface value is about 0.6, but if about 20% of the mass were volatile organics, then this ratio would be about 0.8 and equivalent to leg average values reported by these authors. No significant change in the ratio is evident during L2 at low altitude, while the greater scatter at higher altitude is often caused by aerosol

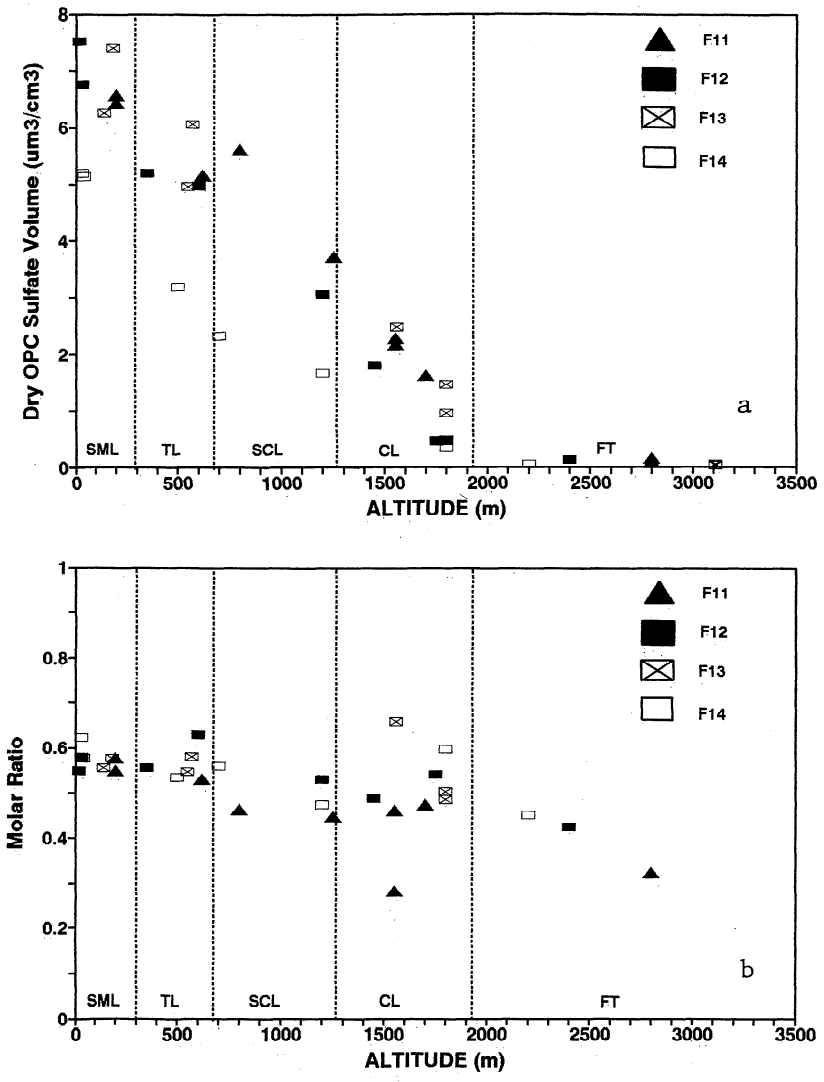

Figure 4. Vertical profiles of (a) inferred OPC sulfate volume and (b) the inferred ammonium to sulfate molar ratio obtained from OPC data during L2. Data were selected from similar locations relative to balloon (see text) and layers identified as in Figure 1. Note the slightly lower values for molar ratio in SCL and CL compared to SML and TL.

variability over the sampling intervals. The generally higher values of the ratio at lower altitude may reflect a surface source of ammonia during the recent history of the air mass.

3.3. CN Evolution

We selected CN as the primary aerosol data for a comparison of aerosol evolution since it is the most continuous aerosol measurement and, as shown above, characteristic of the pollution aerosol variability. In order to minimize uncertainties associated with aerosol variability over a leg, we have focused on the evolution of a subset of the data illustrated in Figure 2. The complexity of the five layer column (Figure 1) is simplified to three layers. The lower layer (LL) includes the SML and TL and the upper layer (UL) includes the SCL and CL with the FT retained as the third layer. Both the LL and UL are represented by the data in Figure 2 even though our data are consistent with the more complex structure. It is presumed that averages of measured data grouped in these two layers should reflect the simpler behavior modeled here. The data selected for comparison is for about a 10 minute interval from each leg located in the more "stable" portion of the pollution plume east of the projected balloon position and indicated by the length and direction (flight orientation) of the dashed arrow in Figure 2. If spikes in the CN data revealed sustained particle shatter from droplets during that period (A.D. Clarke et al., submitted manuscript, 1995), that portion of the interval was excluded.

These averages of CN were then calculated for all legs of L2, and the resulting data are shown in Figure 5 as a time series during L2. The vertical bars associated with the data are based upon uncertainties due to (1) variability in the CN over each interval, (2) the effects of a vertical gradient due to different sample altitudes, (3) uncertainties in position due to the projected balloon location. The representative altitudes the LL (0-700 m), UL (1400-1900 m), and FT (2200-3300 m)) most common to each Lagrangian flight are indicated by a solid uncertainty bar, while less representative altitudes are indicated by a dashed bar. There is a clear tendency for lower values for each successive flight at all altitudes.

Unlike aerosol mass or BC that tend to be conserved in the absence of precipitation, the CN can coagulate with each other and result in lower number concentrations over time. The

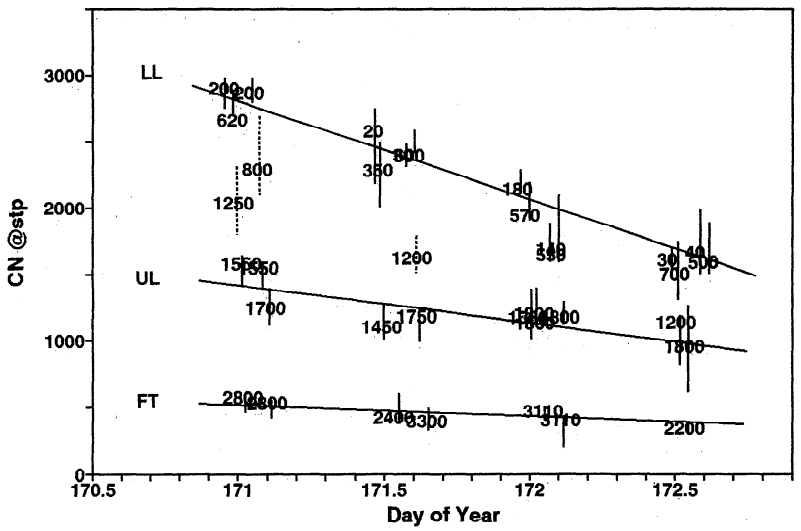

Figure 5. Time series of averaged CN concentration decrease over L2. Vertical bars reflect CN variability over "best" selected sample location relative to balloon including estimates of effects of sampling from different altitudes and other variability (see text). Solid lines are for altitudes that are most representative of the "layer" data shown in Figure 2, while dashed lines are for altitudes that are from less comparable altitudes. Lines are hand drawn to obtain a "representative" reference slope for each altitude for comparison to model results.

coagulation process depends upon a number of factors, including the size distribution and concentration. To estimate this loss, we have selected a typical DMA size distribution observed in the most polluted surface mixed layer during the beginning of L2 and examined its evolution over time using the MAEROS2 coagulation model [*Gelbard and Seinfeld*, 1990]. Mass is conserved in this sectional model. We used 20 sections to characterize the size distribution, and Figure 6 shows the modeled evolution of the size distribution. We infer that for the 34-hour duration of L2 there would be about a 15% decrease in number concentration in the LL (about 10% per day) due to diffusive coagulation. Similar calculations for the lower concentrations aloft result in coagulation rates for the UL of about 6% per day. Both rates will decrease as concentrations drop over time. Because CN are not conserved during coagulation, the time rate of change of CN concentrations is expected to exceed those of either BC or aerosol mass over the L2 period.

With this in mind, we can compare the evolution of the CN with that of both fine-particle OPC mass ($0.15<D_p<0.5$ μm) and BC. The fine-particle sulfate mass concentrations were inferred from our OPC volatility data [*Clarke*, 1991] (also, A.D. Clarke et al., sumitted manuscript, 1995a). Insufficient DMA data exist over the L2 period to carry out an effective comparison with that instrument. Due to the several minutes required to collect an OPC size distribution, the opportunity to select a preferred period is much more limited than for the case of CN. Typically, about three OPC volatility sequences were

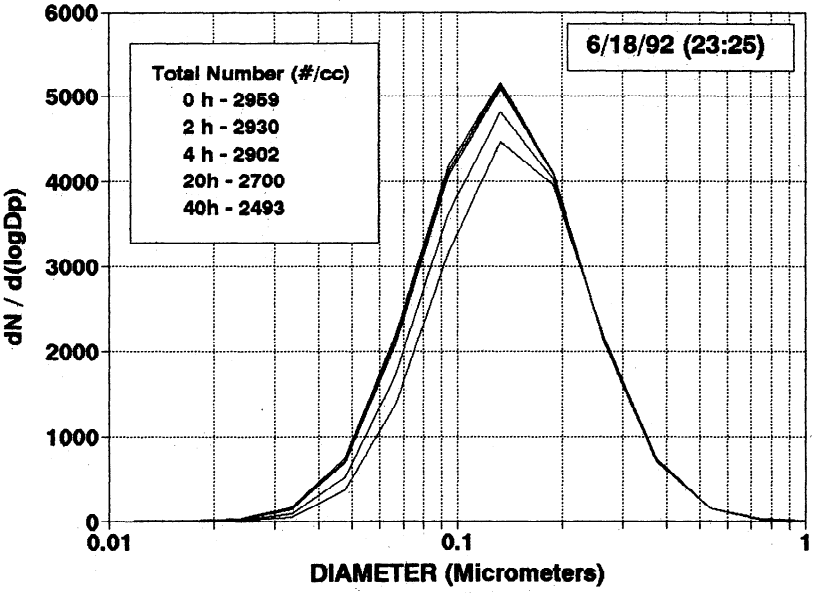

Figure 6. Example of a surface layer DMA size distribution for the CN during June 18, the first day of L2, and the results of the MAEROS model coagulation expected for CN as a function of time over the L2 period.

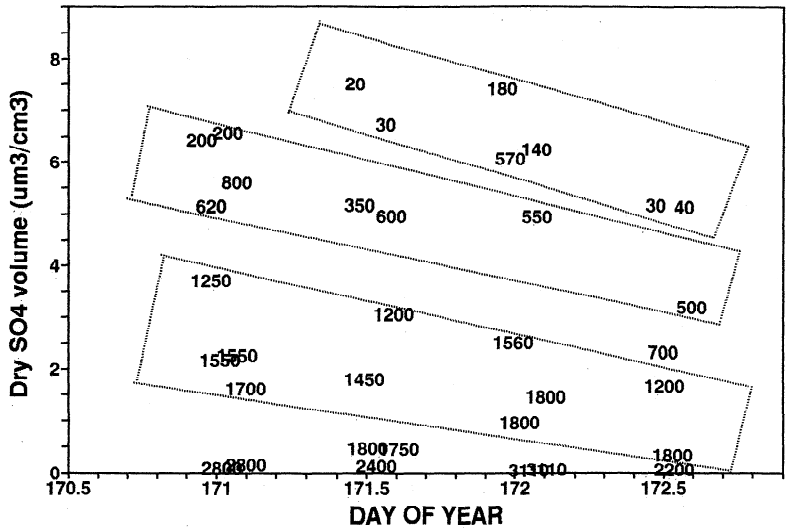

Figure 7. Time series of OPC inferred dry volume collected over similar periods used for CN in Figure 5 and plotted for corresponding altitudes indicated in meters. Boxes have been manually drawn around similar altitude groups in order to draw attention to the temporal decrease in the volume for related altitude ranges.

carried out during the cross-wind part of each leg, and we have selected the one or two closest to the CN sample period for comparison here.

Figure 7 shows the OPC sulfate data for all four flights in L2 as a function of time. Generally, greater scatter is evident for these data than suggested by the CN data shown previously and reflects the atmospheric variability discussed in conjunction with Figure 3. Both gradients in the SML and the small-scale layering in the TL mentioned above as well as the horizontal inhomogeneities often seen in the CN (Figure 2) contribute to the variability. In order to facilitate a comparison to the CN data, we have added trend lines that we believe best reflect the concentration change over time for the approximate altitude range. The decrease in concentration with altitude is evident and a decrease over time is apparent at each altitude.

The same procedure has been used for the BC values obtained for each leg (Figure 8). Because BC is a differential measurement and because both concentration dependent as well as pressure dependent corrections have to be applied (A.D. Clarke et al., submitted manuscript, 1995a), BC is a less precise measurement. Even so, the BC data are broadly consistent with the OPC data and exhibit similar trends. If we look at the change in the best estimate of column average of BC and OPC data we get a decrease to about 65-70% of the original concentrations over the 34-hour period. This trend is also consistent with that observed for average sulfate mass integrated over several flight legs presented elsewhere [*Zhuang and Huebert*, this issue]. Hence the evolution of CN reflects the similar evolution of aerosol mass and the combustion-derived BC in the pollution plume over the L2 period.

The effect of in-cloud processing of CN has not been considered above due to the complexity and uncertainty in trying to simulate this for the decoupled MBL. However, we argue that this effect is likely to be small. First, due to marked

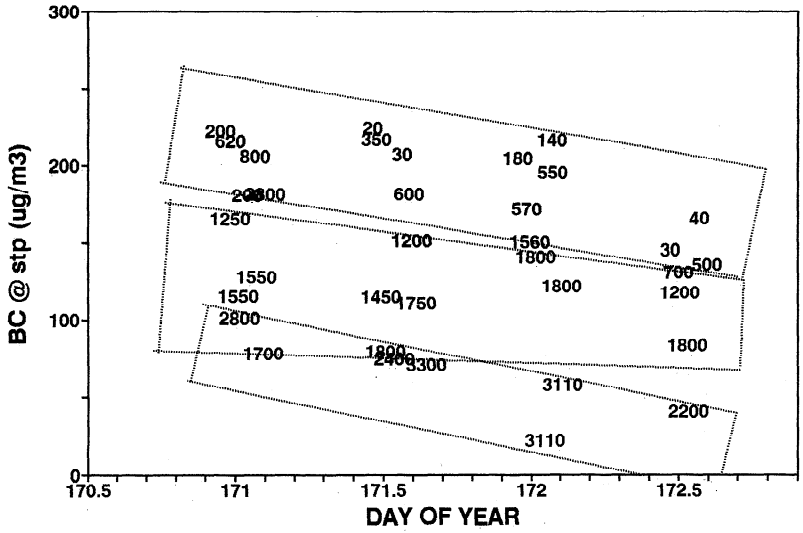

Figure 8. Similar to Figure 7, but for BC. The longer leg averaging time required for BC and greater instrument uncertainty (see text) results in greater scatter here than for Figures 5 and 7.

growth of these aged nuclei (Figure 6) in cloud at about 100% RH, their diffusive loss will be small due to low diffusion coefficients. At the same time, the observed occurrence of drizzle is expected to remove activated CN through collision and coagulation as a result of differential fall speeds. Since drizzle formation was light and appeared not to have reached the ground [*Bretherton et al.*, 1994], the removal of aerosol mass or BC by this mechanism is considered negligible. However, the relative decrease in CN (Figure 5), after allowing for the above-mentioned diffusive loss in cloud-free air, is similar to that of OPC mass and BC (Figure 7 and 8). Hence a significant additional loss of CN through collision/coalescence is not evident, and we assume that this loss is small compared to the primary processes responsible for the observed decrease in mass, BC, and CN.

3.4. Entrainment Model

Based upon the above arguments, the removal of aerosol by precipitation did not appear to be significant during L2 [*Bretherton et al.*, 1994]. Dry deposition, for the aerosol sizes discussed here, is also negligible [*Zhuang and Huebert*, this issue]. The only remaining influence that can reduce concentrations of all species throughout the column below the inversion is entrainment of air with lower concentrations from above the UL/FT inversion. Various estimates of the entrainment rate for L2 have been made based upon European Center for Medium-range Weather Forecasting (ECMWF) analysis of vertical motion, calculation of a water budget and the ozone flux jump method [*Bretherton et al.*, 1994]. Based upon their analysis, the best estimate of the entrainment rate, W_e, presented by these authors is 0.6 ± 0.3 cm s^{-1}.

In order to evaluate the role of entrainment on aerosol evolution for the decoupled multilayer system present during ASTEX, we must consider the mechanisms that exchange material between the layers. Two significant inversions exist, one near 700 m capping the LL, and a stronger one near 1900 m between the UL and FT. Analysis of the thermodynamic structure [*Martin et al.*, 1994] suggests that turbulent and shear driven entrainment across both inversions is present. They also find that "blobs" of convective surface air mix up from and rise up to the inversion near 1800 m with little mixing and feed the stratocumulus. Hence the evolution of the aerosol includes the meteorologically driven processes of entrainment across both inversions, mixing within the layers and plume convection from the surface to cloud level. The relatively small change in the L2 inversion heights over time, in spite of this entrainment, is also indicative of compensating horizontal divergence [*Bretherton et al.*, 1994].

Here we use the observations above to examine the role of entrainment on aerosol evolution. Our assumptions for the simulation of the CN evolution in the three layers include the following.

1. CN concentrations (C_o) above the primary inversion can be specified as a function of time from our observations.
2. No production of new nuclei occurred during L2.
3. The time evolution of CN at a representative altitude in the UL (see Figure 5) can be used to represent the mean evolution of the UL even though it is not generally as "well mixed" as the LL.
4. The first-order linear slopes to the CN data shown in Figure 5 can be used to test the modeled evolution of CN concentration in the UL and LL (identified as C_u and C_l, respectively).
5. Coagulation loss based upon Figure 6 and adjusted for the decreasing concentrations over L2 can be estimated at about 7.2% per day in the LL and a somewhat lower 4.3% per day in the UL due to the lower concentrations present there.
6. Mixing of FT aerosol into the UL can be specified with a subsidence entrainment rate W_o. We will examine our model with the values of 0.6 ± 0.3 cm s^{-1} for W_o determined for L2 [*Bretherton et al.*, 1994].
7. A nearly constant height can be used for the primary inversion of H=1900 m and the height of the LL at H_l=600 m. Sounding data for the region [*Martin et al.*, 1994] suggest some variation in H_l due to time variability in convective plumes leaving the LL and mixing with the UL, however, a long term trend is not evident during L2 [*Bretherton et al.*, 1994].
8. The horizontal divergence in response to W_o is distributed equally over the UL and LL.
9. The entrainment rate between the LL and UL can be represented as a subsidence component and a mixing component. The mean subsidence component is a consequence of mass conservation (and 7 and 8 above) and is given as the product of W_o and H_l / H. An additional mixing entrainment term, $W_e = W_d(\text{down}) = W_u(\text{up})$, is used to reflect equal mixing between the UL and LL such that there is no contribution to divergence in either layer due to this mixing.

An illustration of the box model and relevant components is found in Figure 9. For suitably small time steps (dt), we used the above constraints to allow the specification of concentrations in each layer of the column in terms of the concentration at the previous time step and using the values for the FT concentrations, C_o, obtained form the straight line fit to the FT data shown in Figure 5. CN concentrations for the UL and LL can be written as differential equations for both UL and LL, where C_u, C_l, C_o are concentrations in UL, LL, and FT; k_u and k_l are coagulation loss rates in UL and LL.

$$dC_u/dt = -k_u C_u + \{W_o(C_o - C_u) + W_e(C_l - C_u)\} / H_u$$

$$dC_l/dt = -k_l C_l + \{W_o(H_l/H) + W_e\}(C_l - C_u) / H_l$$

Although we have described W_e as a mixing term, we do not mean to imply that this describes only the process of small-scale turbulent mixing at the boundary of the UL and LL. This approach is also taken to allow for the possible entrainment of

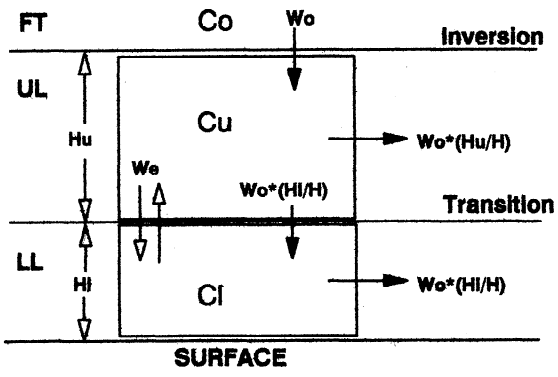

Figure 9. Illustration of box model used to examine Lagrangian CN evolution.

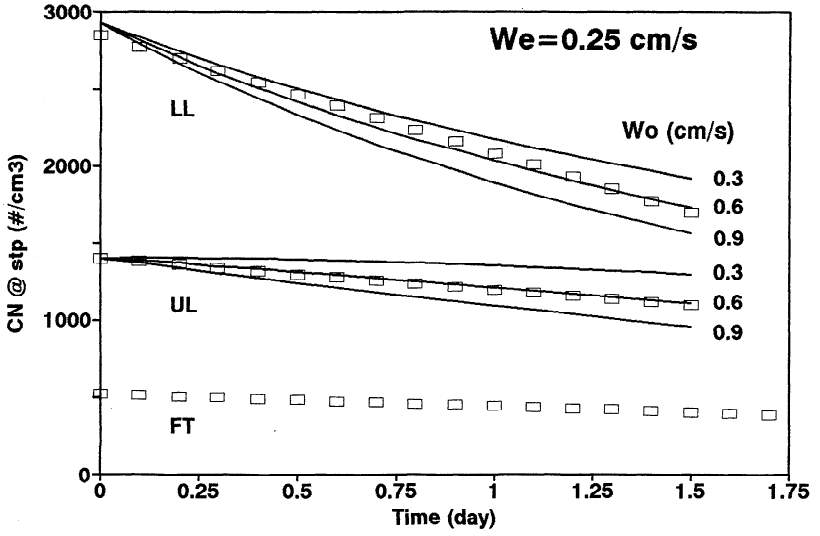

Figure 10. Model results for CN evolution in the three layer model (solid lines) compared to linear reference fit taken from Figure 5 (open squares) for entrainment values discussed in text.

more air into the LL than simply that required to maintain the assumed constant values for H and H_l (i.e., W_o*H_l/H). The observed plume convection of LL air to the top of the UL [*Martin et al.*, 1994] is one mechanism that would require the additional entrainment term W_e if the above conditions/assumptions are to be maintained (e.g., equal divergence in the LL and UL). Alternate and more complex approaches might be considered but they cannot be tested with the data we have available.

Figure 10 reveals the behavior of the above model for various choices of W_o and W_e (solid lines) as compared to our estimated "best fit" to the CN data shown in Figure 5 (open squares). The values of W_o illustrated (0.3, 0.6, and 0.9 cm s^{-1}) correspond to the "low," "best," and "high" values determined for L2 from three independent methods [*Bretherton et al.*, 1994]. The value of W_e was adjusted until the best fit for CN evolution was achieved for both the UL and LL. For the "best" value of W_o=0.6 cm s^{-1} this was found to occur for W_e=0.25 cm s^{-1}. For the "high" and "low" cases of W_o it was not possible to find a W_e that could simultaneously satisfy the "best fit" (Figure 5) evolution of CN in the UL and LL consistent with the constraints described above. For example, in order to lower the LL line for "low" entrainment of W_o=0.3 cm s^{-1}, we must employ a higher W_e which raises the "fit" for the UL line further away from the observed data. Similar difficulties arise when the "high" value is tried. This suggests that values for W_o and W_e are constrained by the CN data and our model and that the "best" values indicated are appropriate within about ± 20% for the conditions described.

If we assume that the W_e component is completely accounted for by the convective flux of cumulus plumes out of the boundary layer then the effective entrainment rate into the LL is the sum of $W_o*(H_l/H)$ and W_e = 0.2+0.25 cm/s=0.45 cm/s. The mean detrainment of LL air though cumulus plumes due to W_e=0.25 cm/s from the LL of depth 600 m corresponds to a loss of LL air to the UL of about 200 m d^{-1}. This provides an estimate of the role of buoyant plumes from the surface mixed layer in feeding surface aerosol and moisture, etc., to the UL cloud layer during L2. This estimate would be lower if appreciable contributions to W_e are only due to mixing exchange across the LL/UL boundary.

4. Horizontal CN Variability and Mixing

The CN data (Figure 2) reveal that L2 was carried out near a marked gradient in aerosol concentrations from east to west. The behavior of the RCN/CN ratio characterized during a more extensive measurement of a similar gradient region on the day before L2 [*Clarke et al.*, this issue] provides some insight to the process probably influencing the CN data shown in Figure 2. In this adjacent clean air this ratio was only about 0.2 and similar to observations in clean air reported previously over the Pacific [*Clarke*, 1993]. We suggest that the combined changes in CN concentrations and the RCN/CN ratio can be used to infer information on the mixing and evolution of aerosol types. In Figure 2 we see that the cross-wind (pollution) legs have a ratio near 0.8, the same as found for the pollution air mass 3 days earlier. The ratio can be seen to be a few percent higher in the SML than aloft in the SCL. In view of the entrainment discussed above and the gradual decrease to lower RCN/CN values aloft (A.D. Clarke et al., submitted manuscript, 1995) it is reasonable to expect the small decrease in the ratio at any given altitude that is evident in Figure 2. The overall decrease in CN over time (Figure5) for this small change in the RCN/CN ratio also shows that no significant production of "new" (volatile) nuclei occurred in the pollution air mass during L2 since this would substantially increase the number of volatile CN and lower the ratio.

It is also of interest to examine the behavior of CN and the ratio for the gradient region at the west end of the legs in Figure 2. The change in RCN/CN values in the SML for the first three flights is relatively small and averages only about 5%, 4%, and 3% for flights 11, 12, and 13, respectively. A more pronounced change is evident in RCN/CN ratio in Figure 2 for flight 14 where it shows a marked decrease from about 0.75 to 0.64, or a change of about 17%. All nuclei concentrations at the west end of this leg are seen to drop by a factor of 2 from the concentrations on the east end. This suggests a mixing of aerosol with different RCN/CN ratios and concentrations (e.g., clean air and polluted air).

We explore this hypothesis by supposing this mixing occurs in the absence of removal and examine the resulting changes in the ratio for consistency with values expected for the mix. We

assume that the boundary layer CN concentrations and RCN/CN ratio (given above for surface clean air measured 3 days before) continue to be representative at about 200 cm^{-3} and 0.2 respectively. Hence the expected fraction (F) of polluted air (CN=C_p=1600) mixed with clean air (CN=C_c=200) to yield an observed mix (CN=C_m=625) (see west end Figure 2, flight 14 in SML) can be determined from

$$C_p F + C_c (1-F) = C_m$$

or $1600F + 200(1-F) = 625$ to yield F=0.30. Similarly, the expected RCN/CN ratio for the mix (R_m) predicted from the ratios R_c=0.2 and R_p=0.74 observed for clean and polluted regions can be written for the RCN as

$$1600 FR_p + 200 (1-F)R_c = 625 R_m$$

to yield R_m = 0.64. This is the same as the observed ratio (Figure 2) and supports the proposed mixing of two different air masses with different RCN/CN ratios. We argue for mixing, since such large excursions in the ratio are not observed with concentration changes in the body of the plume and would not be expected here as a consequence of precipitation scavenging. Precipitation was both low during L2, and for this internally mixed aerosol [*Clarke et al.*,this issue) it would likely remove CN and RCN as the same particle and should only have a small resulting effect on the ratio. A similar calculation applied to the smaller changes evident for flight 11 (with R_p=0.8 and R_c=0.2) suggests a value of F=0.74 and R_m=0.78. The observed value of R_m is slightly lower at about 0.76. This could indicate that other than just mixing may be involved (e.g., precipitation effects) or simply reveals a limitation of this approach when the RCN/CN ratios only change by small amounts.

The above considerations suggest that the RCN/CN ratio may serve as a "conservative" and rapid tool for the identifying the relative mixing of air masses with sufficiently different ratios (e.g., polluted and clean marine) and may allow discrimination between concentration changes arising from mixing versus precipitation scavenging. Use of this ratio is most effective in cases like this where an aged pollution aerosol with the relatively low coagulation rate (estimated here about 7% per day) and high RCN/CN ratio interact with clean air having a low ratio. Recognizing and interpreting such mixing can be important to the assessment of plume evolution.

5. Conclusion

We view this first attempt at a detailed Lagrangian evolution experiment as a success in spite of the difficulty in evaluating this complex data set. Although the avoidance of this complexity would benefit analysis of future Lagrangian missions, the decoupled layers present during L2 may well be typical conditions in many regions and constitute an environment we will be compelled to understand. In spite of these difficulties, our data suggest that the evolution of the European plume during ASTEX L2 was marked by (1) the absence of formation of new nuclei, probably due to the large surface area available for heterogeneous processes; (2) a low coagulation rate due to an already aged distribution and absence of smaller nuclei; (3) the reduction in concentrations driven primarily by entrainment from the free troposphere; and (4) an evolution constrained by decoupled layers below the inversion.

The evolution of CN was consistent with a two-layer decoupled system with entrainment through the main inversion of about 0.6 cm s^{-1} and entrainment into the lower decoupled region of about 0.45 cm s^{-1}, if equal divergence is assumed for each layer. Possible compensating convective plume detrainment out of the 700-m-thick lower layer up to cloud level is estimated at about 0.25 cm s^{-1}, or about 200m d^{-1}. This mechanism would also help maintain specific humidity at cloud level in spite of entrainment of drier air from above. Due to the significance of the entrainment term, we emphasize that an adequate characterization of this term will be essential for the interpretation of similar Lagrangian evolution.

Interpretation of changes in aerosol character (e.g., concentration changes due to removal versus mixing) may require "conservative" aerosol parameters that can be compared to other conservative air mass indices. We have provided examples of how the ratio of RCN/CN might be used in this fashion to improve our understanding of the mixing between different air masses. Other ratios such as black carbon to sulfate might serve similar purposes, but due to longer integration times and uncertainties arising from both sampling and interpretation of instrument performance, they are often less effective for aircraft application.

We emphasize that the above results reflect properties averaged over the 36-hour L2 period. The meteorological and aerosol fields are more complex than suggested by this averaged behavior. Short-term changes in inversion heights, water vapor mixing ratios and gradients, layer thicknesses and clouds measured by the various aircraft platforms [*Martin et al.*, 1994] reflect both temporal changes in these features and spatial structure in the L2 air mass. These include periods where either "direct entrainment" into the LL or the alternate "mixing" described between the UL and LL appear to be consistent with observed water vapor gradients between the layers. Without a more complete description of the meteorological and aerosol fields (e.g., three -dimensional lidar, radar), we feel that the "average" approach taken above is the most appropriate.

Acknowledgments. We thank the many people that contributed to making the ASTEX/MAGE experiment a success and particularly the crew and staff of the NCAR Research Aviation Facility who worked with us aboard the Electra. Special appreciation is extended to Barry Huebert, who championed the cause of the Lagrangian experiment and worked hard to implement it. Appreciation is extended to Zhibian Li for her assistance and comments during manuscript preparation. This research is a contribution to the International Global Atmospheric Chemistry (IGAC) Core project of the International Geosphere-Biosphere Programme (IGBP). Our participation was supported by funds from the Office of Naval Research under grant N00014-92-J-1388. SOEST contribution 3946.

References

Air and Waste Management Association, *Aerosols and Atmospheric Optics, Proceedings of the International Specialty Conference on Radiative Balance and Visual Air Quality (Snowbird, Utah)*, Pittsburgh, Pa., 1994.

Benkowitz, C.M., C.M. Berkowitcz, R.C. Easter, S. Nemesure, R.Wengener, and S.E. Schwartz, Sulfate over the North Atlantic and adjacent continental regions: Evaluation for October and November 1986 using a three-dimensional model driven by observation derived meteorology, *J. Geophys. Res.*, *99*, 20,725-20,756, 1994.

Bretherton, C.S. and R. Pincus, Cloudiness and marine boundary layer dynamics in the ASTEX Lagrangian experiments, Part I, Synoptic setting and vertical structure, *J. Atmos. Sci.*, 52, 2,707-2,723, 1995.

Bretherton, C.S., P. Austin, and S.T. Siems, Cloudiness and marine boundary layer dynamics in the ASTEX Lagrangian experiments, Part 2, Cloudiness, drizzle, surface fluxes and entrainment, *J. Atmos. Sci.*, 52, 2,724-2,735, 1995.

Businger, S., S. Chiswell, W.C. Ulmer, and R. Johnson, Balloons as a Lagrangian platform for atmospheric research", *J. Geophys.Res.*, this issue.

Charlson, R.J., J.E.Lovelock, M.O.Andreae, and S.G. Warren, Oceanic phytoplankton, atmospheric sulfur, cloud albedo and climate, *Nature*, 326, 665, 1987.

Charlson, R.J., S.E. Schwartz, J.M. Hales, R.D. Cess, J.A. Coakley Jr., J.E. Hansen, and D.J. Hofmann, Climate forcing by anthropogenic aerosols, *Science*, 255, 423-430, 1992.

Clarke, A.D., A thermo-optic technique for in situ analysis of size resolved aerosol physicochemistry, *Atmos. Environ.*, *25A*, 635-644, 1991.

Clarke, A.D., Atmospheric nuclei in the Pacific midtroposphere: Their nature, concentration and evolution, *J. Geophys. Res.*, 98 (D11), 20,633-20,647, 1993.

Clarke, A.D., J.N. Porter, F.P.J. Valero, and P. Pilewski, Vertical profiles, aerosol microphysics and optical closure during the Atlantic Stratocumulus Transition Experiment: Measured and modeled column optical properties, J. Geophys. Res., this issue.

Galloway, J.N., G.E. Likens, W.C. Keene, and J.M. Miller, The composition of precipitation in remote areas of the world, *J.Geophys. Res.*,*87*, 8771-8786,. 1982.

Galloway, J.N., The deposition of sulfur and nitrogen from the remote atmosphere, in *The biogeochemical cycling of sulfur and nitrogen in the remote atmosphere*, edited by J.N. Galloway, R.J. Charlson, M.O. Andreae, and H. Rhode, pp143-175, D. Riedel, Dortrecht, Holland, 1985

Gelbard, F., and J.H. Seinfield, Simulation of multicomponent aerosol dynamics, *J. Colloid Interface Sci.*, *78*, 485-501, 1990.

Huebert, B.J., A. Pzenny and B. Blomquist, The ASTEX/MAGE experiment, *J. Geophys. Res.*, this issue.

Martin, G.M., D.W. Johnson, D.P. Rogers, P.R. Jonas, P.Minnis, and D.A. Hegg, Observation of the interaction between cumulus clouds and warm stratocumulus clouds in the marine boundary layer during ASTEX, *J. Atmos. Sci.*, 52, 2902-2922, 1994.

Penner, J.E., et al., Quantifying and minimizing uncertainty of climate forcing by anthropogenic aerosol, *Rep. DOE/NBB-0092T*, Natl. Tech. Inf. Serv., U.S. Dep. of Commerce, Springfield, Va., 1993.

Zhuang, L., and B.J. Huebert, A Lagrangian analysis of the total ammonia budget during the Atlantic Stratocumulus Transition Experiment/Marine Aerosol and Gas Exchange, *J. Geophys. Res.*, this issue.

A.D. Clarke, J.N. Porter, and T. Uehara, School of Ocean and Earth Science and Technology, University of Hawaii, 1000 Pope Rd., Honolulu, HI, 96822, email: tclarke@soest.hawaii.edu; porter@soest.hawaii.edu; uehara@soest.hawaii.edu

(Recieved May 9, 1995; revised August 4, 1995; accepted August 5, 1995)